Selection of Fluorinated Aptamer Targeting RNA Element with Different Chirality

Yuliya Dantsu, Ying Zhang and Wen Zhang*

Department of Biochemistry and Molecular Biology, Indiana University School of Medicine, Indianapolis, IN 46202

Melvin and Bren Simon Cancer Center, Indianapolis, IN 46202, USA

E-mail: wz15@iu.edu

RNA aptamer, Fluorination, Chirality

ABSTRACT: The development of RNA aptamers with high specificity and affinity for target molecules is a critical advancement in the field of therapeutic and diagnostic applications. This study presents the selection of a 2'-fluoro modified mirror-image RNA aptamer through the in vitro SELEX process. Using a random RNA library, we performed iterative rounds of selection and amplification to enrich aptamers that bind specifically to the viral frameshift element which contains the opposite chirality. The unnatural chirality of the aptamer improved its enzymatic stability, and the incorporation of 2'-fluoro modifications was crucial in enhancing the binding affinity of the aptamers. After nine rounds of SELEX, the enriched RNA pool was cloned, sequenced, and analyzed, revealing a dominant aptamer sequence. The selected 2'-fluoro modified mirror-image RNA aptamer demonstrated a dissociation constant of approximately 1.6 μM, indicating moderate binding affinity with the target and exceptional stability against nuclease degradation. Our findings highlight the potential of 2'-fluoro modified mirror-image RNA aptamers in enhancing the stability and utility of RNA-based therapeutics and diagnostics, paving the way for future applications in diverse biomedical fields.

RNA aptamers, short single-stranded RNA molecules capable of folding into versatile three-dimensional geometries and binding to specific target molecules with high affinity and selectivity, have emerged as versatile tools with numerous applications in biotechnology, medicine, and diagnostics[1]. The selection of RNA aptamers with desired properties typically involves iterative rounds of in vitro evolution, a process known as SELEX (Systematic Evolution of Ligands by EXponential enrichment). SELEX allows for the identification of aptamers that can recognize a wide range of targets, including proteins, small molecules, and even whole cells, with high affinity and specificity[2]. Traditional RNA aptamers, however, are susceptible to degradation by nucleases, limiting their stability and utility in various biological applications[3]. To date, tremendous efforts have been devoted targeting nucleic acid structures to engender the stable candidates in biological fluids[4].

One useful strategy to overcome the limitation of stability is to apply the mirror-image RNA aptamers, wherein the ribose sugars of the RNA backbone are replaced with L-ribose, rendering them resistant to nuclease degradation while retaining their binding properties. This mirror-image approach not only enhances the stability of RNA aptamers but also expands the potential applications of RNA-based therapeutics and diagnostics. So far, the L-nucleic acids-based aptamers have been isolated to target disease-related elements, including small molecules[5], non-coding RNAs[6], amino acids[7] and proteins[8]. All these L-aptamers were observed to have exceptional affinities and greatly improved stability. They could bind to the selective targets through unique tertiary structural features and block the disease-related biological metabolism activities. Given their particularities, these L-aptamers might be further explored and used as future advanced therapies.

In this study, we report the selection and characterization of a new mirror-image RNA aptamer using in vitro SELEX. The target molecule for aptamer selection is the attenuator hairpin structure of coronaviruses, a critical regulatory element that controls the frameshift mechanism of virus gene expression. All coronaviruses, including severe acute respiratory syndrome (SARS)-CoV-2, utilize the essential programmed -1 ribosomal frameshifting (-1 RF) strategy to regulate the RNA genome expression in the 2 overlapping translational open reading frames (ORF 1A and ORF 1B, Figure 1A)[9]. In the -1 RF mechanism, the cis-acting elements in the mRNA can direct elongating ribosomes to shift the reading frame by 1 nucleobase toward the 5′-direction[10]. The stable and structured RNA frameshifting element (FSE) controls the unique -1 RF. FSE is composed of three elements, including attenuator hairpin (AH), slippery site and pseudoknot (Figure 1A). They can collectively function to prohibit the initiation of frameshifting, thereby altering the protein coding on viral mRNA. Among FSE RNA structures, the attenuator hairpin is located immediately 5′ of the slippery site, and it regulates -1 RF by attenuating its activity[11]. The primary sequence and predicted secondary structure containing AGCU tetraloop and bulges are shown in Figure 1B[12, 13].

Therefore, the controlling of gene expression by FSE is critical for viral replication and pathogenesis[14]. One attractive way to inhibit the viral frameshifting and interfere the viral replication is to develop the structure-specific binder to target the FES element. There have been drug-like small molecules identified to selectively bind to the AH structure and impair the frameshifting of virus[12, 15]. These studies demonstrated the

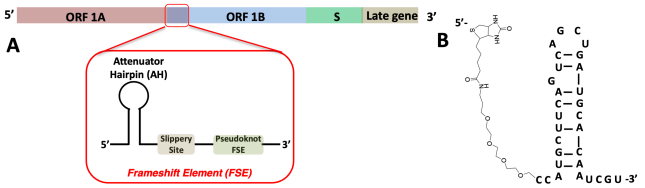

Figure 1. (A) Schematic representation of SARS-CoV-2 RNA genome. The location of the viral frameshift element was indicated by the red box. (B) The sequence and predicted secondary structure of the attenuator hairpin, which is biotin labeled as the SELEX target.

promise that the RNA genome of SARS-CoV-2 could be an ideal drug targets to disrupt the viral cellular functions. The future development of the structure-specific ligands to target virus genome could be based on small molecules or other macromolecules, which has the potential to serve as the complementary strategy of COVID-19 vaccine. Overall, by targeting this regulatory element with RNA aptamers, it is expected to modulate frameshifting dynamics and disrupt the production of essential viral proteins, thereby inhibiting viral replication and reducing viral pathogenicity.

In addition, fluorination is a prevalent chemical derivatization extensively utilized in pharmaceutical chemistry. This is attributed to the distinctive biophysical and biochemical properties of fluorine, such as its small atomic size and high electronegativity[16]. Particularly, when replacing the H or OH group by fluorine element in nucleic acid drugs, the small size of fluorine leads to minimal steric effect on nucleic acid functions, and the significant electronic effect of fluoride modification could lead to the characteristic pseudo hydrogen bonding, as well as the alteration of nucleic acid sugar pucker and overall structures[17]. Thus, fluorination has become popular approach in nucleic acid-based therapeutics, including anticancer and antiviral nucleosides[18], and fluoride-oligonucleotides as therapeutic antisense[19], siRNA[20] and aptamer[21] drugs. In our lab, the 2′-F-derivatized L-pyrimidines have been successfully synthesized[22], and it was discovered that the fluoride atom contributed to rigidify the L-ribose to enhance the helical structural and thermal stability[23], engender the pseudo-hydrogen bonds and strengthened stacking interactions[24]. Therefore, we attempt in this study to further expand the application of 2′-fluoro-L-nucleic acids by isolating the functional mirror-image aptamer, which has enhanced stability and binding affinity, thus improving its potential as a therapeutic agent against viral infections.

Due to the lack of DNA and RNA polymerases capable of recognizing mirror-image molecules, our SELEX was completed in a mirror-image manner (Figure 2A). In order to select L-aptamers that can bind to naturally occurring D-type RNA, the target molecule in the actual SELEX was L-type, while the aptamers selected in each round were based on D-type. Therefore, the biotin-labeled L-type target molecule, L-RNA attenuator hairpin (L-AH, Figure 1B), was synthesized by solid-phase synthesis and used as the target molecule in each round, tightly binding to streptavidin molecules on magnetic beads to select functional aptamer sequences. Random DNA library was synthesized by IDT, and the random region was composed of 45 nucleotides flanked by 5' and 3' primer regions (Figure 2B). At the primer regions, T7 promoter binding sequence was included for the in vitro transcription. The 5′ and 3′ primer for PCR and in vitro transcription was 5′-TTCTAATACGACTCACTATA GGTTACCAGCCTTCACTGC-3′ and 5′-GTGTGACCGAC

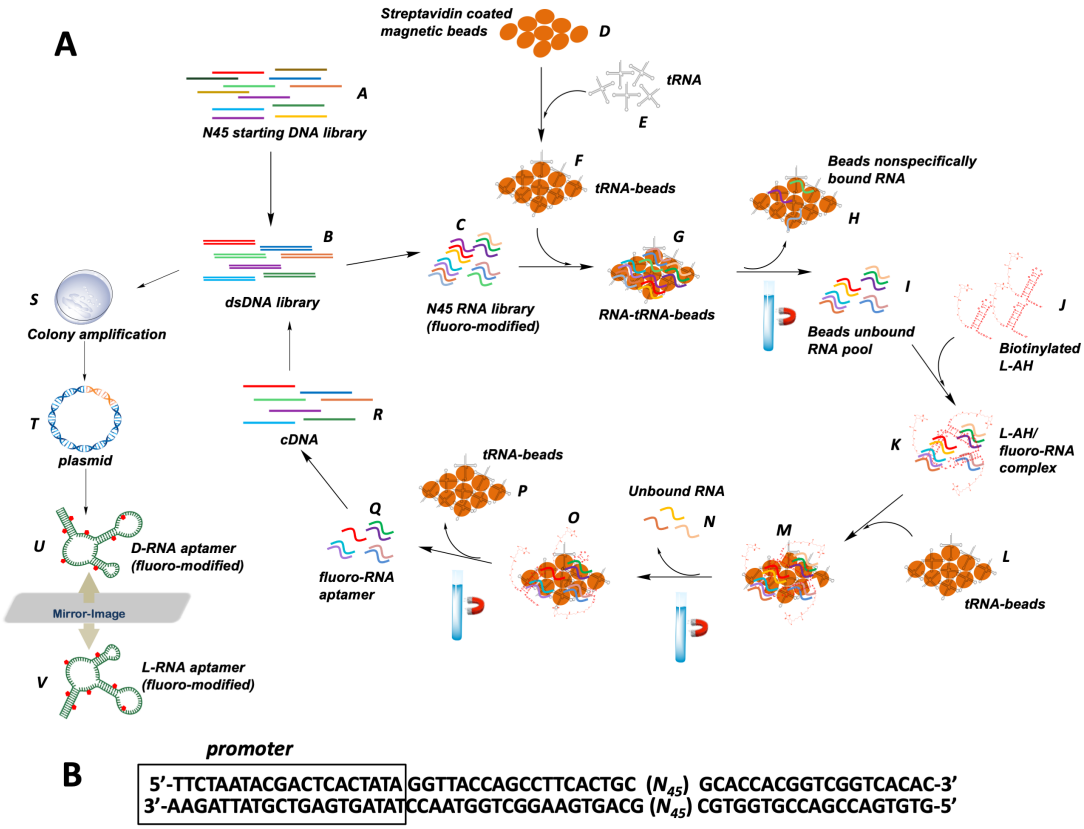

Figure 2. (A) Schematic representation of the mirror-image SELEX. (B) The sequence of dsDNA library in each round. The promoter region for T7 RNA polymerase recognition was boxed.

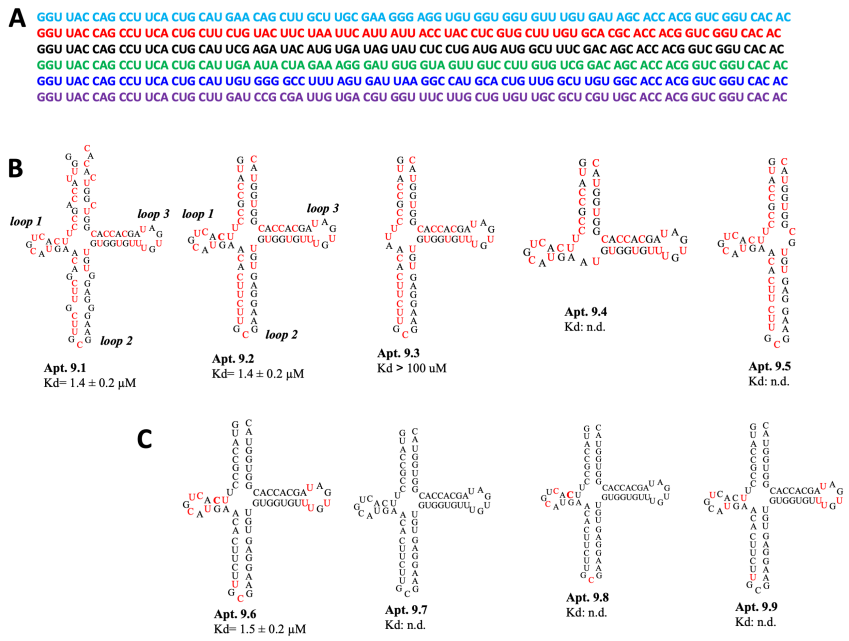

Figure 3. (A) The sequences of 5 enriched aptamers after nine rounds of in vitro selection. (B) The predicted secondary structure of Apt. 9.1, as well as its truncated versions, 9.2, 9.3, 9.4 and 9.5. (C) The predicted secondary structure of the functional aptamer Apt. 9.6, Apt. 9.7, Apt. 9.8, and Apt. 9.9, which contains limited number of fluoro modifications. In all the secondary structures, fluoro modified resides are labeled by red color, and the Kd values are listed below the structures.

CGTGGTGC-3′, respectively. In the first round, 1 nmol random RNA library was prepared by in vitro transcription, using the Y639F T7 RNA polymerase mutant. In each round, the streptavidin coated dynabeads were first incubated with 0.1 mg/ml yeast tRNA for 2 hours at room temperature to block the non-specific binding. The reaction mixture containing the RNA library and the corresponding buffer conditions was heated at 80 ºC for 2 min, then slowly cooled to room temperature to form the RNA structure. The negative selection was first performed by incubating the RNA library with the prepared dynabeads for certain time. The supernatant was extracted and used for the following positive selection. In the positive selection, the 5′-biotinylated L-AH was added to the reaction mixture and incubated with the RNA library for certain time. Then, the reaction was added to a 1 mg of the prepared dynabeads and incubated for additional an hour. The supernatant was discarded, and the dynabeads were washed twice using the washing buffer. The captured RNAs were eluted with 100 µl of elution buffer containing 25 mM NaOH and 1 mM EDTA, followed by neutralization with Tris-HCl buffer (pH 7.5) and purification with NEB RNA clean and concentration column. The process of selection and amplification was then repeated with the selection stringency progressively increased each round by employing longer wash times and decreasing template concentrations and incubation times (Table S1).

The enriched RNA library was then reverse transcribed using NEB ProtoScript® II Reverse Transcriptase. After reverse transcription, the RNA library was degraded by adding 10 µl of 1M NaOH solution and incubated at 95 ºC for 10 min. The obtained cDNA single-stranded template was PCR amplified using the forward and reverse selection primers, and NEB Q5® High-Fidelity DNA Polymerases. The subsequent dsDNA template was used for the mutant T7 in vitro transcription for the next round. Overall, we did nine rounds of selection in this study, and the enriched ssDNA template were PCR amplified to introduce an A-tail for effective ligation and TOPO vector transformation using Invitrogen TOPO-TA cloning kit. The bacteria were grown at 37 ºC for overnight. Single colonies were picked, and PCR amplified, followed by plasmid extraction and Sanger Sequencing by Genewiz.

From the Sanger sequencing results, six most enriched representative sequences were identified (Figure 3A). A representative of the candidates (Apt. 9.1) was presented in Figure 3B. Using RNA secondary structure prediction program Mfold[25], the secondary structure of Apt.9.1 was predicted, which consisted of 83 nucleotides, cloverleaf-like structure, 4 stems and 3 loops (Figure 3B). Microscale thermophoresis (MST) binding assays were performed by measuring the binding affinity of the aptamer to the synthesized 5′-FAM labeled L-AH. The K_d of Apt. 9.1 was measured to be 1.4 µM. The 2′-fluoro-modified uridine and cytidine residues are located in all stems and loops.

The 5′ and 3′ primer regions of the aptamer were initially designed as fixed sequences for PCR amplification and T7 transcription purposes. However, when we attempted to truncate the primer region for a shorter aptamer, the binding affinity was totally lost. Finally, we obtained a 71nt truncated Apt. 9.2 by deleting the bulges and flanking nucleotides, which maintained the K_d of 1.4 µM as binding affinity. To investigate which loop/stem regions contributed to the aptamer binding, we then synthesized 3 truncated aptamers (Apt. 9.3, 9.4 and 9.5), and one loop/stem section was deleted in each aptamer mutant. It was discovered that, when loop 1 was truncated, Apt. 9.3 presented much weaker binding affinity (K_d >100 µM). When loop 2 or loop 3 was truncated, no binding affinity could be measured in Apt 9.4 and 9.5. This result indicates the importance of all three RNA loops, which may fold into compacted three-dimensional conformation by interacting each other.

One more important question is whether the fluoride modifications contribute to the aptamer folding and binding, due to its unique electronegativity and ability of forming inter- and intramolecularly hydrogen bonds. We then chemically synthesized the mutated chimeric aptamer Apt. 9.6, which contained the 2′-

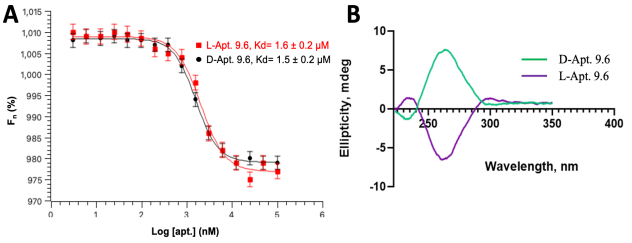

Figure 4. (A) Binding curve in MST assays generated from the difference in initial fluorescence intensity compared to the intensity in the presence of heat. D-Apt. 9.6 against FAM-L-AH (black), and L-Apt. 9.6 against FAM-D-AH (red) are presented. The error bars represent the standard deviation of 3 independent replicates. (B) Normalized CD spectra of D- and L-type aptamers Apt 9.6.

fluoride modified cytidine and uridine residues in all three loops, and the wild-type uridine and cytidine residues in the stem regions. The K_d of this aptamer was measured to be 1.5 μM, which suggests that the 2′-fluoro-modifications in the stem regions don't present significant contribution to the RNA folding and aptamer binding. The function of those fluoride atoms were likely the modest enhancement of thermostability of RNA duplex, which had been observed before[22]. We then attempted to replace all the 2′-fluoro-pyrimidines with native residues, and found the aptamer mutant, Apt. 9.7, entirely lost the binding affinity. Similarly, when only 2′-fluoro modified cytidines or 2′-fluoro modified uridines were introduced in the aptamer (Apt. 9.8 and Apt. 9.9), no binding affinity could be detected, which indicated the importance of those 2′-fluoro modifications. When the wild-type 2′-OH groups were replaced with 2′-F atoms, the original hydrogen bonding patterns likely changed and the electronegativity of fluoride could cause local disturbance of sugar pucker conformation, all leading to the destabilization of the aptamer cloverleaf structure.

We then investigated and compared the binding affinities between D-Apt. 9.6 with L-AH versus L-Apt. 9.6 with D-AH. We found them to be similar to each other, with the K_d to be 1.5 ± 0.2 and 1.6 ± 0.2 μM (Figure 4A). The difference between the two binding affinities could be due to the different qualities of chemicals in the solid-phase syntheses. We then performed the circular dichroism studies to characterize the chiralities of the two aptamers. The corresponding spectra are shown in Figure 4B. The data revealed that the D-form 2'-F-modified Apt. 9.6 adopted a structure containing a high positive band at 266 nm and a weak negative band at 236 nm, which was generated by the characteristic A-form duplexes in the aptamer. In contrast, the chiral inversion of L-Apt. 9.6 displayed a high negative band at 266 nm and a weak positive band at 236 nm. The data illustrates the two synthetic aptamers have the mirror-image conformations as the chiral counterparts.

In this study, we successfully identified an L-RNA aptamer capable of binding to a native RNA element, demonstrating significant potential for therapeutic and diagnostic applications. Our findings indicate that the 2'-fluoro modifications within the L-RNA aptamer play a crucial role in its binding affinity, although the binding observed was modest rather than exceptionally strong. Moreover, comparative analysis with non-modified aptamers revealed that the introduction of 2'-fluoro groups improves binding strength and specificity towards the target RNA element, albeit not to the desired extent. These results align with previous studies that have shown the stabilizing effects of 2'-fluoro modifications in RNA-based therapeutics. To further enhance the binding affinity, we plan to explore other modifications such as 2'-methoxy groups, which our lab has successfully synthesized in the past[26]. Preliminary evidence suggests that 2'-methoxy modifications could offer even greater stability and binding efficiency due to their superior resistance to nucleases and improved structural rigidity.

However, it is important to note that while the in vitro binding characteristics are promising, in vivo efficacy and potential immunogenic responses need to be thoroughly evaluated in future studies. Additionally, exploring the structural dynamics of the L-RNA aptamer in complex with the native RNA element through advanced techniques such as X-ray crystallography or NMR spectroscopy could provide deeper insights into the binding mechanism.

Overall, our research highlights the potential of 2'-fluoro modified L-RNA aptamers as a foundational step towards developing robust tools for targeting native RNA elements. Further modifications, including the incorporation of 2'-methoxy groups, are anticipated to enhance these properties, paving the way for the development of novel RNA-based therapeutics and diagnostic agents.

ASSOCIATED CONTENT

The Supporting Information is available free of charge at xxx

AUTHOR INFORMATION

Corresponding Author

*Wen Zhang-Department of Biochemistry and Molecular Biology, Indiana University School of Medicine, Indianapolis, IN 46202, USA; orcid.org/0000- 0003-4811-4384; Email: wz15@iu.edu

Notes

The authors declare no competing financial interest.

ACKNOWLEDGMENT

We thank the Zhang lab for helpful discussions, insightful commentary and careful revision of the manuscript. We thank Dr. L. Zeng and the Chemical Genomics Core at IUSM for the help.

REFERENCES

(1) Saenger, W. *Principles of nucleic acid structure*; Springer Science & Business Media, 2013. Keefe, A. D.; Pai, S.; Ellington, A. Aptamers as therapeutics. *Nat. Rev. Drug Discov.* **2010**, *9* (7), 537-550.

(2) Wilson, D. S.; Szostak, J. W. In vitro selection of functional nucleic acids. *Annu. Rev. Biochem.* **1999**, *68* (1), 611-647.

(3) Shigdar, S.; Macdonald, J.; O'Connor, M.; Wang, T.; Xiang, D.; Qiao, L.; Wei, M.; Zhou, S.-F.; Zhu, Y.; Kong, L. Aptamers as theranostic agents: modifications, serum stability and functionalisation. *Sensors* **2013**, *13* (10), 13624-13637. Zhou, J.; Rossi, J. Aptamers as targeted therapeutics: current potential and challenges. *Nat. Rev. Drug Discov.* **2017**, *16* (3), 181-202.

(4) E Wang, R.; Wu, H.; Niu, Y.; Cai, J. Improving the stability of aptamers by chemical modification. *Curr. Med. Chem.* **2011**, *18* (27), 4126-4138.

(5) Klussmann, S.; Nolte, A.; Bald, R.; Erdmann, V. A.; Fürste, J. P. Mirror-image RNA that binds D-adenosine. *Nat. Biotechnol.* **1996**, *14* (9), 1112-1115. Luo, X.; Chen, Z.; Li, H.; Li, W.; Cui, L.; Huang, J. Exploiting the application of l-aptamer with excellent stability: an efficient sensing platform for malachite green in fish samples. *Analyst* **2019**, *144* (14), 4204-4209. Feng, X.-N.; Cui, Y.-X.; Zhang, J.; Tang, A.-N.; Mao, H.-B.; Kong, D.-M. Chiral interaction is a decisive factor to replace d-DNA with l-DNA aptamers. *Anal. Chem.* **2020**, *92* (9), 6470-6477. Chen, H.; Xie, S.; Liang, H.; Wu, C.; Cui, L.; Huan, S.-Y.; Zhang, X. Generation of biostable L-aptamers against achiral targets by chiral inversion of existing D-aptamers. *Talanta* **2017**, *164*, 662-667.
(6) Sczepanski, J. T.; Joyce, G. F. Specific inhibition of microRNA processing using L-RNA aptamers. *J. Am. Chem. Soc.* **2015**, *137* (51), 16032-16037. Dey, S.; Sczepanski, J. T. In vitro selection of l-DNA aptamers that bind a structured d-RNA molecule. *Nucleic Acids Res.* **2020**, *48* (4), 1669-1680. Kabza, A. M.; Sczepanski, J. T. An l-RNA Aptamer with Expanded Chemical Functionality that Inhibits MicroRNA Biogenesis. *ChemBioChem* **2017**, *18* (18), 1824-1827. Sczepanski, J. T.; Joyce, G. F. Binding of a structured D-RNA molecule by an L-RNA aptamer. *J. Am. Chem. Soc.* **2013**, *135* (36), 13290-13293. Umar, M. I.; Kwok, C. K. Specific suppression of D-RNA G-quadruplex–protein interaction with an L-RNA aptamer. *Nucleic Acids Res.* **2020**, *48* (18), 10125-10141. Chan, C. Y.; Kwok, C. K. Specific Binding of ad-RNA G-Quadruplex Structure with an l-RNA Aptamer. *Angew. Chem. Int. Ed.* **2020**, *132* (13), 5331-5335.
(7) Nolte, A.; Klußmann, S.; Bald, R.; Erdmann, V. A.; Fürste, J. P. Mirror-design of L-oligonucleotide ligands binding to L-arginine. *Nat. Biotechnol.* **1996**, *14* (9), 1116-1119. Ravelet, C.; Boulkedid, R.; Ravel, A.; Grosset, C.; Villet, A.; Fize, J.; Peyrin, E. A L-RNA aptamer chiral stationary phase for the resolution of target and related compounds. *J. Chromatogr. A* **2005**, *1076* (1-2), 62-70. Brumbt, A.; Ravelet, C.; Grosset, C.; Ravel, A.; Villet, A.; Peyrin, E. Chiral stationary phase based on a biostable L-RNA aptamer. *Anal. Chem.* **2005**, *77* (7), 1993-1998. Ruta, J.; Ravelet, C.; Grosset, C.; Fize, J.; Ravel, A.; Villet, A.; Peyrin, E. Enantiomeric separation using an l-RNA aptamer as chiral additive in partial-filling capillary electrophoresis. *Anal. Chem.* **2006**, *78* (9), 3032-3039. Ruta, J.; Grosset, C.; Ravelet, C.; Fize, J.; Villet, A.; Ravel, A.; Peyrin, E. Chiral resolution of histidine using an anti-D-histidine L-RNA aptamer microbore column. *J. Chromatogr. B* **2007**, *845* (2), 186-190.
(8) Hoehlig, K.; Maasch, C.; Shushakova, N.; Buchner, K.; Huber-Lang, M.; Purschke, W. G.; Vater, A.; Klussmann, S. A novel C5a-neutralizing mirror-image (l-) aptamer prevents organ failure and improves survival in experimental sepsis. *Mol. Ther.* **2013**, *21* (12), 2236-2246. Chakraborty, S.; Winkelmann, V. E.; Braumüller, S.; Palmer, A.; Schultze, A.; Klohs, B.; Ignatius, A.; Vater, A.; Fauler, M.; Frick, M. Role of the C5a-C5a receptor axis in the inflammatory responses of the lungs after experimental polytrauma and hemorrhagic shock. *Sci. Rep.* **2021**, *11* (1), 1-15. Citro, A.; Pellegrini, S.; Dugnani, E.; Eulberg, D.; Klussmann, S.; Piemonti, L. CCL 2/MCP-1 and CXCL 12/SDF-1 blockade by L-aptamers improve pancreatic islet engraftment and survival in mouse. *Am. J. Transplant.* **2019**, *19* (11), 3131-3138. Eulberg, D.; Purschke, W.; Anders, H.-J.; Selve, N.; Klussmann, S. *Spiegelmer NOX-E36 for renal diseases*; Royal Society of Chemistry, 2008. Fischer, M. J.; Schmidt, J.; Koulchitsky, S.; Klussmann, S.; Vater, A.; Messlinger, K. Effect of a calcitonin gene-related peptide-binding L-RNA aptamer on neuronal activity in the rat spinal trigeminal nucleus. *J. Headache Pain* **2018**, *19* (1), 1-9. Olea Jr, C.; Weidmann, J.; Dawson, P. E.; Joyce, G. F. An L-RNA aptamer that binds and inhibits RNase. *Chem. Biol.* **2015**, *22* (11), 1437-1441.
(9) Bhatt, P. R.; Scaiola, A.; Loughran, G.; Leibundgut, M.; Kratzel, A.; Meurs, R.; Dreos, R.; O'Connor, K. M.; McMillan, A.; Bode, J. W. Structural basis of ribosomal frameshifting during translation of the SARS-CoV-2 RNA genome. *Science* **2021**, *372* (6548), 1306-1313. Brian, D.; Baric, R. Coronavirus genome structure and replication. *Coronavirus Replic. Reverse Genet.* **2005**, 1-30.
(10) Jacks, T.; Varmus, H. E. Expression of the Rous sarcoma virus pol gene by ribosomal frameshifting. *Science* **1985**, *230* (4731), 1237-1242.
(11) Cho, C.-P.; Lin, S.-C.; Chou, M.-Y.; Hsu, H.-T.; Chang, K.-Y. Regulation of programmed ribosomal frameshifting by co-translational refolding RNA hairpins. *PLOS ONE* **2013**, *8* (4), e62283.
(12) Kelly, J. A.; Olson, A. N.; Neupane, K.; Munshi, S.; San Emeterio, J.; Pollack, L.; Woodside, M. T.; Dinman, J. D. Structural and functional conservation of the programmed− 1 ribosomal frameshift signal of SARS coronavirus 2 (SARS-CoV-2). *J. Biol. Chem.* **2020**, *295* (31), 10741-10748.
(13) Rangan, R.; Zheludev, I. N.; Hagey, R. J.; Pham, E. A.; Wayment-Steele, H. K.; Glenn, J. S.; Das, R. RNA genome conservation and secondary structure in SARS-CoV-2 and SARS-related viruses: a first look. *RNA* **2020**, *26* (8), 937-959.
(14) Graham, R. L.; Sparks, J. S.; Eckerle, L. D.; Sims, A. C.; Denison, M. R. SARS coronavirus replicase proteins in pathogenesis. *Virus Res.* **2008**, *133* (1), 88-100.
(15) Haniff, H. S.; Tong, Y.; Liu, X.; Chen, J. L.; Suresh, B. M.; Andrews, R. J.; Peterson, J. M.; O'Leary, C. A.; Benhamou, R. I.; Moss, W. N. Targeting the SARS-CoV-2 RNA genome with small molecule binders and ribonuclease targeting chimera (RIBOTAC) degraders. *ACS Cent. Sci.* **2020**, *6* (10), 1713-1721.
(16) Purser, S.; Moore, P. R.; Swallow, S.; Gouverneur, V. Fluorine in medicinal chemistry. *Chem. Soc. Rev.* **2008**, *37* (2), 320-330.
(17) Guo, F.; Li, Q.; Zhou, C. Synthesis and biological applications of fluoro-modified nucleic acids. *Org. Biomol. Chem.* **2017**, *15* (45), 9552-9565.

(18) Qiu, X.-L.; Xu, X.-H.; Qing, F.-L. Recent advances in the synthesis of fluorinated nucleosides. *Tetrahedron* **2010**, *66* (4).
(19) Kawasaki, A. M.; Casper, M. D.; Freier, S. M.; Lesnik, E. A.; Zounes, M. C.; Cummins, L. L.; Gonzalez, C.; Cook, P. D. Uniformly modified 2'-deoxy-2'-fluoro-phosphorothioate oligonucleotides as nuclease-resistant antisense compounds with high affinity and specificity for RNA targets. *J. Med. Chem.* **1993**, *36* (7), 831-841.
(20) Chernolovskaya, E. L.; Zenkova, M. A. Chemical modification of siRNA. *Curr. Opin. Mol. Ther.* **2010**, *12* (2), 158-167.
(21) Kratschmer, C.; Levy, M. Effect of chemical modifications on aptamer stability in serum. *Nucleic Acid Ther.* **2017**, *27* (6), 335-344.
(22) Dantsu, Y.; Zhang, Y.; Zhang, W. Synthesis and structural characterization of 2′-Deoxy-2′-fluoro-L-uridine nucleic acids. *Org. Lett.* **2021**, *23* (13), 5007-5011. Dantsu, Y.; Zhang, Y.; Zhang, W. Synthesis of 2′-Deoxy-2′-fluoro-l-cytidine and Fluorinated l-Nucleic Acids for Structural Studies. *Chem. Select.* **2021**, *6* (39), 10597-10600.
(23) Egli, M.; Pallan, P. S. Crystallographic studies of chemically modified nucleic acids: a backward glance. *Chem. Biodivers.* **2010**, *7* (1), 60-89.
(24) Patra, A.; Paolillo, M.; Charisse, K.; Manoharan, M.; Rozners, E.; Egli, M. 2′-Fluoro RNA Shows Increased Watson–Crick H-Bonding Strength and Stacking Relative to RNA: Evidence from NMR and Thermodynamic Data. *Angew. Chem.* **2012**, *124* (47), 12033-12036. Pallan, P. S.; Greene, E. M.; Jicman, P. A.; Pandey, R. K.; Manoharan, M.; Rozners, E.; Egli, M. Unexpected origins of the enhanced pairing affinity of 2′-fluoro-modified RNA. *Nucleic Acids Res.* **2011**, *39* (8), 3482-3495.
(25) Zuker, M. Mfold web server for nucleic acid folding and hybridization prediction. *Nucleic Acids Res.* **2003**, *31* (13), 3406-3415.
(26) Dantsu, Y.; Zhang, W. Derivatization of Mirror-Image l-Nucleic Acids with 2′-OMe Modification for Thermal and Structural Stabilization. *ChemBioChem* **2023**, *24* (12), e202200764. Dantsu, Y.; Zhang, W. Synthesis and Structural Characterization of 2′-Deoxy-2′-Methoxy-L-Cytidine Nucleic Acids. *ChemistrySelect* **2023**, *8* (29), e202301966.

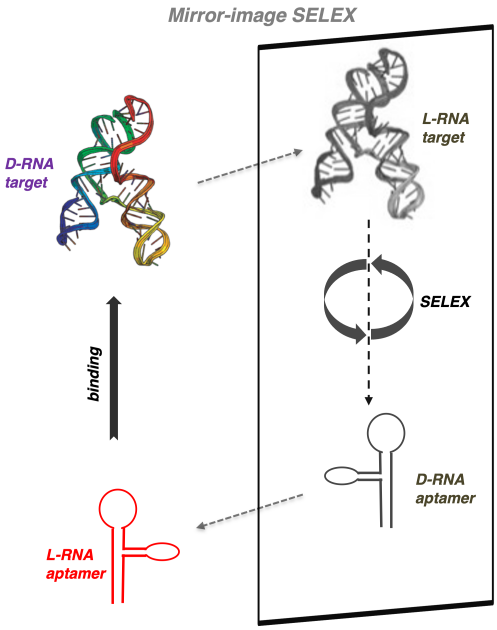
Mirror-image SELEX
D-RNA target
L-RNA target
SELEX
binding
D-RNA aptamer
L-RNA aptamer